Elastic Phase-Strain Distribution in a Particulate-Reinforced Metal-Matrix Composite Deforming by Slip or Creep

MARK R. DAYMOND, CHRISTIAN LUND, MARK A.M. BOURKE, and DAVID C. DUNAND

The macroscopic load-bearing capability of a composite is directly related to the strain partitioning due to load transfer between the component phases. Using neutron diffraction, the elastic mean phase strains were measured during *in-situ* loading of a Cu-15 vol pct Mo particulate metal-matrix composite (MMC) at 25 °C, 300 °C, and 350 °C. The degree of load sharing at each temperature was compared to finite-element (FE) results. The load transfer from the matrix to reinforcement is both qualitatively and quantitatively different at low and high temperatures. When the matrix creeps, load transfer is less effective than when the matrix deforms by slip; also, load transfer at elevated temperatures decreases with increasing applied stress.

I. INTRODUCTION

THE interest in metal-matrix composites (MMCs) in recent years has been motivated by their enhanced properties as compared to the unreinforced matrix, *e.g.*, an improved specific stiffness, strength, and wear resistance and a tailorable coefficient of thermal expansion (CTE).[1] Furthermore, the reinforcing phase of an MMC has a higher creep resistance than the matrix at a given temperature, thus improving the creep properties of the composite as compared to the unreinforced matrix.[2]

At any temperature, the strength of a composite depends both on the level of indirect matrix strengthening (*e.g.*, due to an increased dislocation density or increased precipitation from the presence of the reinforcing phase) and on direct strengthening from load transfer between the matrix and reinforcing phase. These issues are particularly relevant when the reinforcing phase is discontinuous. If a high proportion of the applied load is carried by the reinforcing phase, the composite is efficient. The level of load sharing is dependent on reinforcement volume fraction, shape, and orientation and on the relative elastic properties of the phases.[3] It is reasonable to assume that the partitioning ratio of an applied load between the matrix and reinforcement will remain constant with increasing applied load, provided that both phases remain elastic. However, once the stress levels in the composite (usually in the matrix) are high enough for relaxation or inelastic deformation processes to occur, the load-partitioning ratio changes.

Many models have been developed to predict the load sharing between phases[3,4] of a composite. One approach for evaluating their validity is to measure the mean phase stresses using Bragg (elastic) neutron diffraction.[3,5,6] For example, room-temperature *in-situ* measurements of load partitioning in the phases of discontinuous Al/SiC and Al/TiC MMCs[3,7,8] have shown that, once the aluminium matrix yields, its capability to bear further increases in load is reduced, so that the reinforcing phase carries a greater proportion of the load.

The majority of diffraction-based studies of *in-situ* loading of MMCs reported to date have been carried out at room temperature. However, since many proposed MMC applications involve high temperatures and stresses, a fundamental understanding of the mechanics of creep in these materials is of interest. Only recently have the capabilities at neutron sources progressed to the point that diffraction measurements can be performed *in situ* during creep.[9,10] In this article, we compare the load sharing in a Cu-15 vol pct Mo composite at elevated temperatures (where the copper matrix deforms in a time-dependent manner by creep) to its behavior at room temperature (where plastic deformation by slip of the matrix is time independent).

II. EXPERIMENTAL PROCEDURES

A. *Materials*

A composite consisting of a commercially pure copper matrix, reinforced with pure molybdenum particulates, was fabricated for this study. The Cu-Mo phase diagram shows very little mutual solubility in the solid state and no intermetallic phases.[11] Nevertheless, a strong metallic bond is expected at the Cu-Mo interface, providing good load-transfer characteristics. Cu-Mo composites exhibit a high resistance to mechanical wear and thermally induced deformation, as well as excellent thermal and electrical conduction and a low contact resistance. Although this composite was chosen as a model system, the volume fraction is somewhat lower than, but still comparable to, that used in some commercial Cu-Mo composites for (1) contact material in heavy-duty electrical switching applications, (2) semiconductor thermal management (with tailored CTEs), and (3) resistance welding and electrochemical machining.[12]

The differences between the elastic properties of the matrix and reinforcement are somewhat less in the Cu/Mo system than in the common Al/SiC system (Table I). For a

MARK R. DAYMOND, formerly with the Lujan Center, Los Alamos Neutron Science Center, Los Alamos National Laboratory, is with the ISIS Facility, Rutherford Appleton Lab., Chilton, OX11 0QX, United Kingdom. CHRISTIAN LUND, formerly with the Department of Materials Science and Engineering, Massachusetts Institute of Technology, Cambridge, MA 02319, is with Seagate Corp., Minneapolis, MN 55437. MARK A.M. BOURKE is with the Lujan Center, Los Alamos Neutron Science Center, Los Alamos National Laboratory, Los Alamos, NM 87545. DAVID C. DUNAND, formerly with the Department of Materials Science and Engineering, Massachusetts Institute of Technology, is with the Department of Materials Science and Engineering, Northwestern University, Evanston, IL 60208.

Manuscript submitted November 10, 1998.

Table I. Materials Properties of Copper and Molybdenum

Property	Cu	Mo
Melting point (°C)*	1085	2610
Density (g/cm^3)*	8.93	10.22
CTE at 20 °C (10^{-6}/°C)*	16.5	5
Space group*	*Fm3m*	*Im3m*
Lattice parameter (nm)*	0.361509	0.31468
Elastic modulus (GPa)	125*	324**
Poisson's Ratio**	0.343	0.293

*Ref. 32.
**Ref. 42.

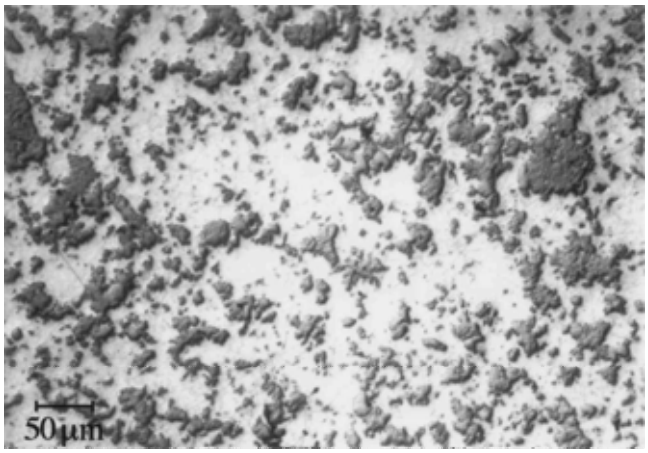

Fig. 1–Optical micrograph of the Cu-15 vol pct Mo composite showing full consolidation, good distribution of the reinforcing phase, and two-phase structure of the particulates. The scale bar shown is 50 μm.

given applied load, the magnitude of elastic strains in the reinforcement is, therefore, larger in the Cu/Mo system, thus offering good strain-measurement sensitivity in both phases. Based on a simple Eshelby calculation,[3,13] a reinforcement level of 15 vol pct was chosen to induce reasonably large strains in both phases, thus optimizing the measurement sensitivity.

Copper composites, with 16.7 wt pct Mo (corresponding to 15 vol pct Mo), and pure-copper control specimens were produced by a powder metallurgy route. The starting materials were 99.9 pct pure, spherical copper powder (Aremco Products, Ossining, NY) less than 44 μm in size, and 99.8 pct pure molybdenum powder (Atlantic Equipment Engineers, Bergenfield, NJ) with a reported size range of 10 to 44 μm. The Cu-Mo powder blend and Cu control powders were packed in steel cans lined with molybdenum foil to prevent contamination by diffusion from the steel. The powders were annealed at 850 °C in a hydrogen atmosphere to reduce any molybdenum or copper oxides. The evacuated, sealed cans were subsequently hot isostatically pressed at 900 °C and 100 MPa for 125 minutes. Tensile specimens, with a gage length of 33 mm and gage diameter of 6.35 mm, were produced by electrodischarge machining.

Figure 1 is a representative optical micrograph of the composite, which shows that very few voids exist in the matrix and that consolidation was effective. This was confirmed by density measurements, which showed approximately 0.3 and 1.1 vol pct of voids in the unreinforced and composite materials, respectively. Figure 1 also shows that the molybdenum particulates are irregularly shaped, approximately equiaxed, reasonably well distributed in the matrix, and with an average size close to the reported lower limit of 10 μm (some individual particulates are in the range of about 1 μm). High-resolution backscattered scanning electron microscope pictures[14] of the densified composites show that the large molybdenum particulates are not, in fact, monolithic, but consist of individual, micron-sized molybdenum particles partially sintered together and separated by a thin layer of copper matrix (some of which is visible in the largest particulates in Figure 1). Thus, the large molybdenum particulates in Figure 1 are, in fact, a fully dense Mo/Cu two-phase structure. The most-likely explanation is that the large molybdenum particulates are partially sintered aggregates of fine, micron-sized molybdenum particles; this is typical of thermal-spray molybdenum powders, which are produced by spray-drying of fine particles to form aggregates, which are then sintered into large particulates. Upon consolidation of the composite, copper was forced into the interparticle space within the particulates. This results in an apparently anomalously high molybdenum volume fraction, if a determination is made from optical micrographs, with each particulate considered to be pure molybdenum.[14]

B. *Measurements*

The use of elastic diffraction techniques to determine changes in lattice parameter, or d spacing (and, thus, elastic strains), is well established[15,16] and is particularly useful for composites, since both phases can be independently and, at a pulsed source, simultaneously examined. Compared to X-rays of the same wavelength, neutrons offer a larger probing depth (*e.g.*, the depth for 50 pct attenuation in copper is about 10 mm for thermal neutrons, while it is about 0.1 mm for X-rays of comparable wavelengths[17]). Thus, neutrons enable the nondestructive determination of bulk volume–averaged strains of each crystalline phase of the material, averaged over a volume, in this case, of about 0.5 cm^3, and in a particular direction determined by the diffraction conditions.[15,16] This bulk averaging removes ambiguities implicit in surface measurements, due to the plane-stress condition. This is especially useful in MMCs, where X-rays from conventional sources can typically only measure reliably the elastic strain in the matrix, since relatively large reinforcements, such as those found in this composite, are rarely found in the outer 0.1 mm layer of the sample. We note, however, that high-intensity, synchrotron X-rays can be successfully used for these types of measurements, as described elsewhere.[14,18]

In-situ load tests were carried out using the neutron powder diffractometer at the Lujan Center (Los Alamos Neutron Science Center at Los Alamos National Laboratory). Unlike a reactor source, where, typically, a monochromatic beam of neutrons is used, the Lujan Center is a pulsed neutron spallation source operating in a time-of-flight mode. Each pulse contains neutrons with a continuous range of velocities and, therefore, wavelengths. By measuring the flight times of the neutrons diffracted by the sample, the wavelength of a detected neutron can be calculated from the de Broglie's relationship. Since the incident neutron beam is polychromatic, all possible lattice planes in an orientation defined by the scattering geometry are recorded simultaneously.

Detectors are placed at fixed angles around the sample, so that the scattering vectors for all reflections recorded in one detector lie in the same direction and, thus, all measure strain in the same direction. Since all lattice planes are recorded, the diffraction spectra from all phases in the composite are measured simultaneously. Strains are recorded relative to the initial state of the system or, if possible, relative to a known stress-free reference sample.

While carrying out fits on single diffraction peaks allows the determination of elastic strain for the corresponding crystallographic direction, it is usual at a pulsed source to average over all the peaks in the spectra using a Rietveld refinement procedure.[19,20] This has been shown to provide a good measure of the bulk average elastic strain.[21,22] We used the Los Alamos Rietveld code GSAS[23] to produce the results described in the following sections. Refinements were carried out between 0.04 and 0.4 nm (0.4 and 4 A) over a total of 55 peaks in the two phases, using the peak-shape function described in References 19 and 20. The effect of *hkl*-dependent intergranular strains due to elastic and plastic anisotropy, and the comparison of Rietveld-determined strains and strains obtained from single-peak fits, is discussed in detail in References 21 and 22.

The load frame used in these experiments was designed for use in the neutron beam. It incorporates universal joints to ensure good uniaxiality of loading and is described in detail elsewhere.[7] Briefly, the loading axis is horizontal and forms an angle of 45 deg to the incident neutron beam, allowing simultaneous measurement in opposing 90 deg detectors of lattice plane spacings parallel to and perpendicular to the loading direction. Each detector is comprised of 31^3 He tubes that subtend an angle of 11 deg in 2θ (from 84.5 to 95.5 deg). Spectra from individual tubes are summed, with corrections for differences in diffraction angle and flight path, to provide a single spectrum for each detector.

The room-temperature operation of the load frame is described in Reference 7, but, in the present experiments, we added two water-cooled radiant parabolic heaters. These are mounted above and below the specimen, out of the neutron flight paths, and produce parallel beams of infrared and visible light 38 mm in width. These heaters provide rapid temperature adjustment in moderate-temperature (150 °C to 700 °C) experiments.[10,24] The sample temperature was monitored using a 0.5-mm-diameter K-type thermocouple placed in a hole in the shoulder of the specimen.[10,12,24] Preliminary tests, using a control sample, showed no detectable temperature gradients (*i.e.*, <0.5 °C) between the specimen shoulder and the irradiated region, after 10 minutes hold at temperature. The temperature at the shoulder was, therefore, considered to be the gage-length temperature and was held to the setpoint temperature within 1 °C throughout the experiments. Boron nitride heat shields were placed on each side of the heaters, with windows that allowed unobstructed passage of the incident and diffracted neutron beams. Due to the limited available space, it was not possible to attach an extensometer to the sample during the high-temperature neutron tests, although one was used during the room-temperature measurements. Conventional creep tests were, therefore, carried out on separate samples outside of the neutron beam, using a dead-weight loading creep frame to determine macroscopic strain rates.

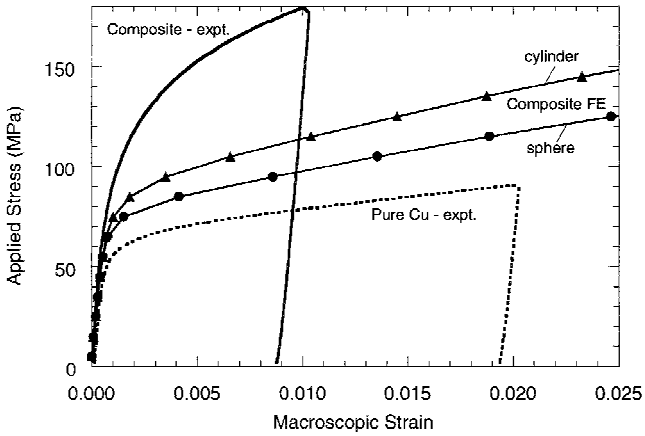

Fig. 2–Room-temperature macroscopic stress-strain response of the unreinforced and composite materials, as measured experimentally and as predicted by the two FE model geometries.

The room-temperature tests were performed at incremental step loads, *i.e.*, the load was raised to a given stress and was held constant under load-control conditions while the neutron measurements were made, then was raised to its next level of stress. Relaxation was noted during the holding times at the highest stresses, as evidenced by some strain accumulation during the hold periods, resulting in a stress-strain curve with less hardening than would have been observed during an uninterrupted tensile test. The macroscopic stress-strain curve shown in Figure 2 indicates the mean elastic strain measured at each applied stress.

A similar procedure was followed for the creep tests, but, in this case, three different samples were used in the 300 °C test to ensure that all measurements were taken during secondary creep, removing any ambiguity caused by the establishment of a steady state during primary creep, or cavitation and necking during tertiary creep. For each specimen, a neutron measurement was made at a low applied load, the load was then increased, and a second neutron measurement made. For the 350 °C test, a single specimen was used for all three elevated loads. We have assumed that strain partitioning is independent of whether the external stress is established in a single step (*i.e.*, a new sample for each applied stress) or incrementally (*i.e.*, one sample for several stresses), provided that tertiary creep does not occur. This behavior is shown by the models described in the following section and in Reference 25. At each new experimental load, neutron-data collection was initiated immediately. However, after primary creep had been exhausted (typically after half an hour), a new set of neutron data was collected for 4 to 5 hours in the secondary creep regime, before increasing the load to the next level. The data collected in the primary regime were poor, due to the short counting times, and only the secondary creep data are reported here.

The models also suggest that strain partitioning should be constant during the secondary creep regime, *i.e.*, once a steady state is reached, the load sharing in the composite is a function only of stress. If this were not the case, an apparent broadening of the peaks would be observed, because a drift of the phase strains during the measurement period causes a shift in the instantaneous position of the diffraction peak. In fact, the peaks at high temperature were slightly narrower than at room temperature (normalized peak widths ~15 pct

smaller). This can be explained by the lower capability of the matrix to maintain stress gradients at elevated temperatures, so that strain broadening of the diffraction peaks was reduced and, in the present case, seems to have compensated for any increase due to thermal broadening.

III. FINITE-ELEMENT MODELING

To model the experiments, finite-element (FE) analysis was carried out using a two-dimensional axisymmetric unit cell with second-order elements. The FE program ABAQUS[26] was used, with mesh generation provided by the PATRAN program.[27] Two reinforcement geometries were considered: spherical and cylindrical (with an aspect ratio of unity). However, the results from the spherical geometry were in poorer agreement with the experiment and, for clarity, are not included in the majority of the figures. Spherical and cylindrical reinforcement geometries give qualitatively the same response, although, quantitatively, the cylindrical system results in a stiffer behavior.[28] Figure 1 shows that most molybdenum particulates are irregular in shape and can, thus, be considered neither spherical nor cylindrical; they often exhibit sharp angles whose stress-concentration effects are better captured by assuming a cylindrical geometry. An increased mesh density near the matrix/reinforcement interface was used to better describe the high stress gradient at the interface,[29] which is important in creep studies because of the high stress sensitivity of the deformation rate. A three-dimensional FE model was also produced to check the validity of the axisymmetric model. The strain-partitioning results obtained for the two- and three-dimensional models in typical calculations were within 5 pct of each other; thus, the results reported are for the two-dimensional model.

The diffraction experiments provide an elastic strain averaged over all the copper and molybdenum present within the sampling volume. Accordingly, to compare the FE results to the diffraction results, it is necessary to carry out a phase-specific average of the strains and stresses over all the elements in the model. A FORTRAN program was written to carry out this averaging on data from the ABAQUS output file.

Initial thermal residual stresses were included in the model prior to loading, by assuming a stress-free temperature of 250 °C (~40 pct of the melting point of the matrix[30]), cooling to room temperature, and then, if appropriate, heating to the testing temperature. Monolithic-phase material properties were used as input parameters (Table I). Elastic and plastic room-temperature data for copper were obtained from tests carried out on the pure-copper control samples and were used as input parameters, assuming kinematic hardening.[26,31] Temperature-dependent values of the elastic modulus, Poisson ratio, yield stress, and creep data were incorporated in the model. The CTEs were obtained from Reference 32. The molybdenum was assumed to be elastic–perfectly plastic,[33] but, due to its high yield stress, it might be expected to remain elastic for all values of the applied stress. In fact, some molybdenum plasticity was noted in the cylindrical-geometry model at high applied stresses in the room-temperature test, due to the high level of constraint on the corner of the cylinder. Copper creep was modeled with a hyperbolic sine law[26,34] incorporating both lattice and core diffusion contributions. At low stresses, this law reduces to low-temperature power-law creep, while, at high stresses, it converges to the power-law breakdown exponential formulation.[26,34] At the temperatures and stresses used in the present experiments, both regimes were expected to be important.[26,34] Even at the highest stress and temperature, the model predicted negligible creep strain in the molybdenum reinforcement, which can, thus, be considered elastic during composite creep.

IV. EXPERIMENTAL AND MODEL RESULTS

A. *Room Temperature*

1. *Macroscopic stress-strain behavior*

Figure 2 shows the experimentally measured room-temperature macroscopic response of the composite and pure-copper standard. Also shown is the predicted macroscopic response using the cylindrical and spherical models (the measured copper macroscopic response was used in the model). The observed Young's modulus of the copper was 121 GPa, compared to the tabulated pure-copper value of 125 GPa (Table I). The measured Young's modulus of the composite was 145 GPa, a 20 pct increase relative to the unreinfored material. In comparison, the FE model predictions for the composite (using the measured 121 GPa copper modulus at room temperature and the reference molybdenum stiffness (Table I)) are 140.5 GPa for the spherical model (a 16 pct increase) and 142.2 GPa for the cylindrical model (an 18 pct increase). A simple volume average gives a stiffness of 151 GPa, the Eshelby (spherical-inclusion) model[1] gives 140 GPa, and a Reuss–Voigt average gives 142.7 GPa (where the Reuss and Voigt limits are 134 and 152 GPa, respectively). While the FE models give a good estimate of the elastic modulus, they significantly underpredict the strain-hardening rate of the composite. Because of the rapid strain hardening, the composite 0.2 pct yield stress (measured at 130 MPa) is double that of pure copper and is also underestimated by the model.

2. *Elastic phase strain behavior*

A room-temperature tensile test was carried out on a Cu-Mo sample *in situ* in the neutron beam. A nominal stress of 5 MPa was used for the initial unloaded measurement to ensure that the specimen was properly aligned. This measurement was taken as the "zero point" of the experiments, for which a reference lattice spacing (d_0) is calculated. All other strains are defined as $(d - d_0)/d_0$ (where d is the measured lattice spacing) and are expressed in units of microstrain ($\mu\varepsilon$), corresponding to a strain of 10^{-6}. The reported strains are, thus, not absolute, since they do not take into account any initial thermal residual stresses caused during fabrication. However, the cylindrical FE model predicted only small initial residual strains at room temperature, which are tensile in the matrix (30 $\mu\varepsilon$) and compressive in the reinforcement (−108 $\mu\varepsilon$); also, the relative changes in phase strains with increasing stress are unaffected. Diffraction measurements were taken at stress increments of 20 MPa up to a maximum value of 165 MPa, with a ramp rate of 20 MPa/min, followed by unloading to 85 MPa and finally to 5 MPa. Each diffraction measurement occurred over a 5-hour period at constant stress.

Room-temperature mean phase strains parallel to the

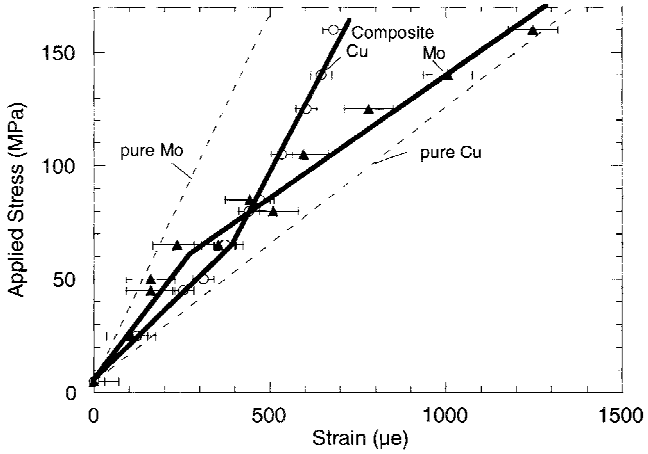

(*a*)

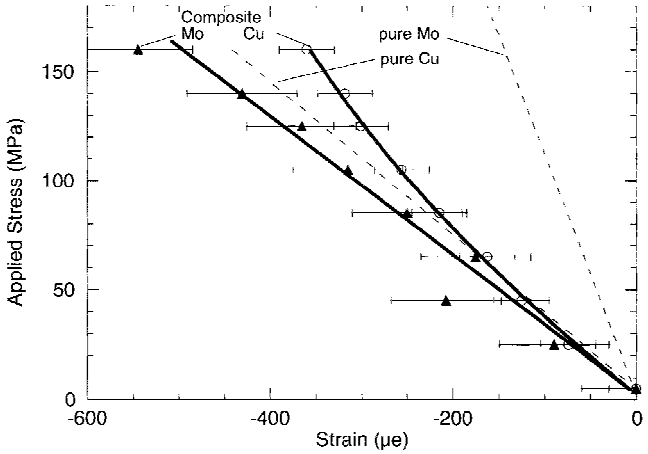

(*b*)

Fig. 3–Elastic phase strain as a function of applied stress at room temperature. Data points were measured by neutron diffraction and lines correspond to the elastic response of pure copper and pure molybdenum: (*a*) parallel to the loading direction and (*b*) perpendicular to the loading direction.

applied load are shown as a function of the applied stress in Figure 3(a). Below 80 MPa, the reinforcement exhibits a lower elastic strain than the matrix. For applied stresses below 70 MPa, the reinforcement and matrix exhibit a linear response, with apparent moduli (slope of applied stress *vs* elastic strain) between the Young's moduli of the individual phases (Table I), as expected from composite-mechanics arguments.[1,3] Since the strains in the molybdenum reinforcement are larger than those in a hypothetical pure molybdenum sample and the strains in the copper matrix are smaller than a hypothetical pure-copper sample, we can infer that load transfer occurs from the compliant copper matrix to the stiff molybdenum inclusions. The experimental scatter shown in Figure 3(a) (± 30 $\mu\varepsilon$ in the copper and ± 70 $\mu\varepsilon$ in the molybdenum) was determined from the average error in lattice parameter calculated from the Rietveld analysis. The larger errors in the molybdenum phase are due to the smaller scattering volume and concomitantly poorer counting statistics. Table II shows that, within experimental scatter, the diffraction data in the elastic range (below an applied stress of 70 MPa) are in agreement with the elastic response of the phases calculated with the elastic FE or Eshelby models.

Table II. Measured and Predicted Elastic Effective Modulus (Ratio of Applied Stress to Elastic Phase Strain, in GPa) in the Elastic Range (<70 MPa) of the Room-Temperature Stress-Strain Curve

Modulus determination	Cu	Mo
Neutron measurement	158	214
FE model (cylinder)	134	208
FE model (sphere)	132	222
Eshelby model	130	235
Pure phase (Table I)	125	324

The strains perpendicular to the applied load are shown in Figure 3(b). While the magnitude of error in the strains is the same as in the axial direction, the relative experimental scatter in the transverse direction is larger because the absolute Poisson strains are smaller. The strains are smaller in the copper matrix than in the molybdenum reinforcement for all applied stresses, in contrast to results in the direction parallel to the applied load. Such a variation can be attributed to Poisson constraints on the phases, although the magnitude of the effect is perhaps surprising. Also shown in Figure 3(b) are the elastic lines of the pure phases, with a slope given by the phase of the Young's modulus divided by its Poisson ratio. As expected from the elastic load transfer observed in the axial direction (Figure 3(a)), the elastic slope of pure molybdenum is steeper than the slope measured in the elastic range for the reinforcement, and *vice versa* for the matrix (Figure 3(b)). Despite the larger error, it is possible to observe subtle deviations from linearity in the transverse copper strains (Figure 3(b)) when macroscopic composite yield occurs, which is in qualitative agreement with the increased load transfer observed in Figure 3(a) in the axial direction.

The experimental measurements are compared to the cylindrical model results in Figures 4(a) and (b). The models shows an initially elastic region, followed by plasticity in the copper at around 70 MPa, which causes the elastic strain curves for the two phases to cross as load is transferred to the molybdenum reinforcement. At higher stresses, a second inflection is seen in the strain response, as the corner of the molybdenum cylinder starts to yield and load transfer to the reinforcement becomes less efficient.

B. HIGH TEMPERATURE

1. *Macroscopic creep behavior*

The minimum creep rates of the composite are plotted as a function of stress in Figure 5, showing a stress exponent (n) of 13 at 300 °C and of 14 at 350 °C. The composite shows lower strain rates and higher stress exponents than those predicted for pure copper deforming by low-temperature power-law creep,[34] with a stress exponent of $(n + 2) = 6.8$, over the examined stress ranges. With data for only two temperatures, any determination of activation energy is doubtful, especially due to the variation in stress exponent with temperature. However, an average value of 211 kJ/mol was obtained, which compares well to values of 117 kJ/mol for core diffusion creep and 197 kJ/mol for lattice diffusion creep[34] for pure copper.

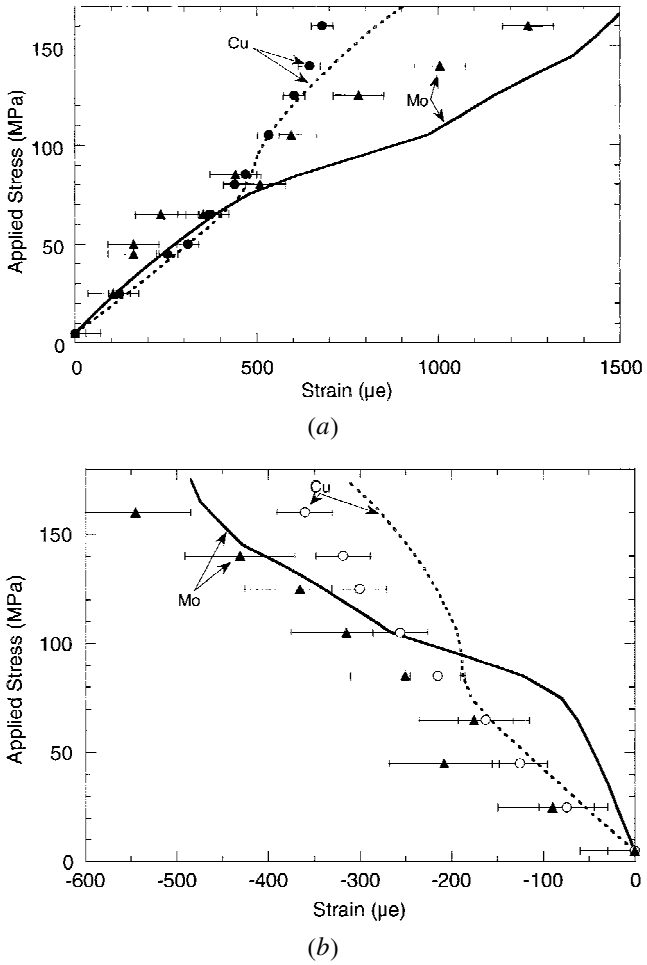

Fig. 4–Elastic phase strain as a function of applied stress at room temperature. Data points were measured by neutron diffraction and the lines were determined from elastic-plastic FE models: (*a*) parallel to the loading direction and (*b*) perpendicular to the loading direction.

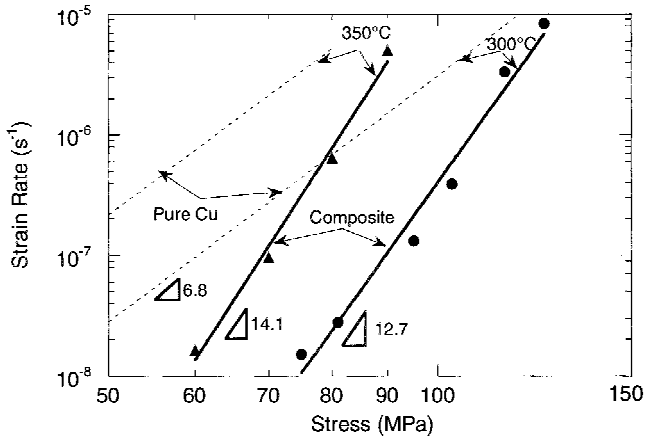

Fig. 5–Creep strain rate as a function of applied stress for 300 °C and 350 °C as determined experimentally for the composites and as calculated for pure copper assuming low-temperature power-law creep.[34]

2. *Elastic Phase-Strain Behavior*

The experimental window for temperature and stress values was determined by the time required (about 5 hours) to obtain a statistically significant neutron measurement of the minority molybdenum phase, coupled with the need to remain within the secondary creep regime. As for the low-temperature tests, a 5 MPa measurement at the appropriate temperature was used as a "zero-strain" reference. Measurements at 300 °C were made at 50, 75, 85, 95, 105, 115, and 125 MPa, and, at 350 °C, measurements were made at 50, 65, and 80 MPa. As mentioned earlier, only two or three stress levels were applied to each sample in the creep regime; the 300 °C measurements at 95, 115, and 125 MPa showed reduced counting statistics, since they were the final load applied to each specimen and were terminated before the expected neutron counts were obtained, due to the onset of the tertiary regime and subsequent sample failure.

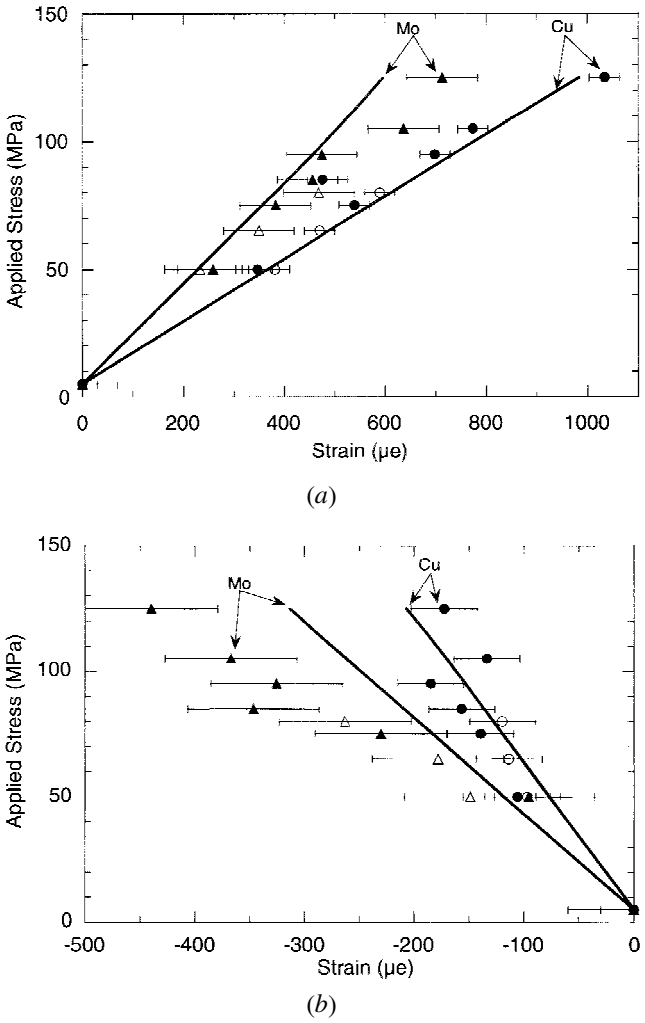

Fig. 6–Comparison between neutron diffraction results and FE models for elastic strain in each phase: (*a*) parallel and (*b*) perpendicular to the loading direction, as a function of applied stress at high temperature. Filled symbols are results from measurements at 300 °C and open symbols from measurements at 350 °C.

The measured phase strains at temperature are plotted in Figures 6(a) and (b). In the axial direction (Figure 6(a)), the copper strains remain larger (more tensile) than for the molybdenum reinforcement, for both the 300 °C and 350 °C tests at all values of applied stress. While experimental results are shown in Figure 5(a) for both temperatures, only the 300 °C model results are shown for clarity, since little difference is observed in the model results between 300 °C and 350 °C. The experimentally observed elastic-strain

development with applied stress in each phase is approximately linear, with perhaps a slight decrease in slope in the copper strains at the highest stress level (125 MPa). In the transverse direction (Figure 6(b)), at both elevated temperatures, the elastic-strain variation with applied stress is also approximately linear.

V. DISCUSSION

A. *Room Temperature*

1. *Macroscopic stress-strain behavior*

While the elastic modulus of the composite is predicted with good accuracy by the FE model, the measured hardening rate is much higher than that predicted (Figure 2). One possible explanation for this discrepancy is that the properties of the copper matrix differ from those of the pure copper, as often reported in MMCs.[1,35] Since the pure-copper control specimens do not show abnormal hardening, the observed behavior in the composite must originate directly or indirectly from the molybdenum phase. The molybdenum particles are, however, too large to significantly increase the matrix hardening rate by (1) reducing the matrix grain size (Hall–Petch hardening), (2) punching mismatch dislocations into the matrix (forest hardening), or (3) interacting with matrix dislocations (Orowan strengthening). Furthermore, any molybdenum oxide (which may have been dissolved in copper and reprecipitated as copper oxide at room temperature) is expected to have been reduced by hydrogen during the annealing treatment prior to consolidation, as H_2O is more stable than MoO_2.[36] Finally, the solubility of molybdenum in copper at the consolidation temperature of 900 °C (which is less than the maximum solubility of 0.06 at. pct Mo at 1083 °C[37]) is too low to induce significant volume fractions of precipitated molybdenum dispersoids.

By far, the most likely reason for the anomalously high hardening rate of the composite is the microstructure of the molybdenum particulates, which consists of two interpenetrating networks of copper and molybdenum, the latter in the form of sintered, micron-sized molybdenum particles. Matrix dislocations can move through the copper within these particulates (whereas they would be blocked by monolithic molybdenum particulates) and interact strongly with the fine molybdenum phase (Orowan mechanism No. 3, as cited previously), leading to locally very high strain-hardening rates.[38] Furthermore, the copper phase within the molybdenum particulates is also expected to be significantly stronger than the copper matrix, due to a fine grain size and large dislocation densities from thermal mismatch upon cooling (mechanisms No. 1 and 2, as cited previously). The latter mechanism was shown to be responsible for the anomalously high rate of strain hardening of Cu-W composites, where tungsten fibers were clustered to volume fractions of about 0.5 during processing.[39]

We also note that the structure of the molybdenum particulates could also be responsible for the high degree of constraint, which would be required in order to explain the relative magnitudes of the transverse phase strains relative to the axial values. Finally, since elastic effects are relatively insensitive to strain hardening in the matrix, the FE models can still be used for elastic predictions and be compared to neutron measurements.

2. *Neutron experiments*

For both phases, the effective modulus departs from the linear value given in Table II once macroscopic composite yielding occurs at a stress of about 80 MPa. For a given increment in applied stress, the increase in the elastic phase strain of the copper matrix becomes smaller, while that in the molybdenum reinforcement becomes larger as compared to the preyield values. This indicates that, when the matrix deforms plastically, the load-partition ratio changes as the reinforcement is preferentially loaded. After subsequent unloading of the composite (not shown), the two phases show residual strains as compared to the initial state: parallel to the loading direction, copper exhibits a compressive strain of $-340 \pm 30\ \mu\varepsilon$, while molybdenum shows a tensile strain of $510 \pm 70\ \mu\varepsilon$. The comparable FE results are -26 and $104\ \mu\varepsilon$ for the spherical model and -238 and $600\ \mu\varepsilon$ for the cylindrical model. The relatively large difference observed between the results from the two models can be attributed to the differing levels of transverse constraint and the resulting degree of plasticity.

Figures 4(a) and 4(b) compare the experimental and FE results for the phase strains of the composite system at room temperature. Approximate agreement is achieved in the axial direction, parallel to the loading axis (Figure 4(a)). However, the calculated slope changes occur at slightly too low an applied stress, *i.e.*, as the stress in the copper reaches a level where macroscopic yielding can occur. Agreement between the models and the experiment is, in general, better at low applied stresses; the increased discrepancy at higher stresses seems to reflect the increased level of hardening measured in the composite compared to the monolithic copper, which has already been discussed in light of the macroscopic stress-strain curves (Figure 2). Before yield, however, the presence of the Mo/Cu two-phase structure does not affect the elastic load transfer between the matrix and reinforcement. As yield occurs and the increased hardening becomes important, the calculated and measured distribution of elastic-phase strains diverge somewhat. This suggests that quantitative agreement between the experiment and model, for both elastoplastic macroscopic strain and elastic phase-strain results, would be improved if a matrix with a higher strain-hardening rate were used in the model, as is indeed observed in preliminary calculations not reported here.

In the transverse direction (Figure 4(b)), agreement between the model (an average of radial and hoop strains) and neutron measurements is, at best, qualitative. The experimental data show an essentially linear relationship between elastic transverse phase strain and applied stress, except for the copper at the highest applied stresses. The initial strain-stress slope is reasonably well predicted for the copper matrix, while the small inflections at higher stress are too small to be verified, given the experimental uncertainty. However, for the molybdenum reinforcing phase, the inflections in the model do not appear experimentally and the predicted initial strain-stress gradient is also too steep. Since the perpendicular strains result from the Poisson effect, the response of the model perpendicular to the applied load is highly dependent on the constraints and boundary conditions imposed (*i.e.*, the particular neighbors of the reinforcement), so that predictions are more susceptible to errors introduced by the use of a unit-cell approach. Finally, residual strains in the transverse direction were measured as 15 ($\pm$40) and

-200 (± 80) $\mu\varepsilon$ for copper and molybdenum, respectively, to be compared to 14 and -75 $\mu\varepsilon$ for the spherical model and 123 and -305 $\mu\varepsilon$ for the cylindrical model. The experimental residual strains are not expected to give a stress balance, since they are relative to the room-temperature state, which is not stress-free because of thermal residual stresses.

B. *High Temperature*

1. *Macroscopic creep behavior*

The composite strain rates obtained from the FE models were higher than those determined experimentally, by between one and two orders of orders of magnitude, and the stress exponent in the composite model was raised by approximately unity relative to that of the unreinforced matrix. This was true for both the spherical and cylindrical geometries and in both the low-temperature power-law regime and the power-law breakdown. Thus, the FE model underpredicted the creep resistance of the matrix and the observed stress exponent. As for the room-temperature experiment, this macroscopic discrepancy can be explained by the presence of the dense Mo/Cu two-phase structure. The molybdenum fine particles strongly inhibit the motion of dislocations in the copper phase within the large particulates, thus decreasing the overall copper creep rate. Thus, the composite can be thought of as a copper matrix containing particulates which are dispersion strengthened, from which a high apparent stress exponent and low creep rate result.[40]

2. *Neutron experiments*

Despite the very poor macroscopic description of the creep rate by the FE models, the elastic strains predicted by the FE models are in reasonable agreement with experiment in the axial direction (Figure 6(a)), capturing at least qualitatively the strain dependence, and the actual elastic strain values are well predicted. In the transverse direction (Figure 6(b)), agreement is slightly poorer. However, the approximately linear response of elastic phase strain with applied stress seems correct, within experimental uncertainty.

The improved agreement between the model and experiment for internal phase strains at high temperature (Figures 6(a) and (b)), as compared to the room-temperature case (Figures 4(a) and (b)), is noteworthy, especially since the FE model does not predict the observed level of improvement in macroscopic-creep strain rate. This suggests that, once a steady state has been reached, the exact rate of creep does not have a major effect on the elastic phase strains. This conclusion is further supported by the fact that the elastic phase strains observed at 300 °C and 350 °C are very similar (both experimentally and in the model), despite the increase in matrix macroscopic creep rate by one order of magnitude (Figure 5).

The stress in the copper matrix at all measured applied stresses is lower at room temperature than at high temperatures. This stress can be estimated as the ratio of the elastic phase strain and the phase Young's modulus (at the appropriate temperature), giving values of 73 and 112 MPa at room temperature and 300 °C, respectively, for an applied stress (σ_a) of 125 MPa. While, in both cases, the molybdenum is acting as a reinforcing phase by lowering the stress in the copper relative to the applied stress, this load transfer is considerably less efficient at high temperatures. Figure 7 shows the fraction of the applied stress measured in the matrix (σ_{Cu}/σ_a) as a function of the applied stress, at both room temperature and 300 °C. In Figure 7, the stresses have been calculated using both the axial strain (ε_1) and transverse strains ($\varepsilon_2 = \varepsilon_3$), assuming that these are the principal strain directions, and using the appropriate stress-strain relation (*e.g.*, Reference 41):

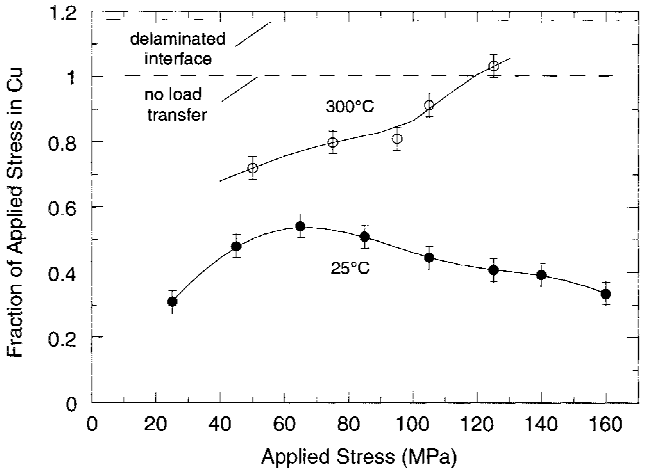

Fig. 7–Fraction of the applied macrostress present in the copper matrix phase parallel to the loading direction, for high- and low-temperature deformation.

$$\sigma_1 = \frac{E\varepsilon_1}{(1+\nu)} + \frac{\nu E(\varepsilon_1 + \varepsilon_2 + \varepsilon_3)}{(1-2\nu)(1+\nu)} \qquad [1]$$

where E is the Young's modulus and ν is the Poisson ratio. This approach is more accurate than the simple ratio mentioned earlier, but introduces larger errors due to the large-percentage scatter in the strains measured in the transverse direction. It is necessary to use the full form of the stress-strain tensor relation, because the constraining (Poisson) effects of the phases on each other mean that the individual phase does not necessarily experience a uniaxial load; it is only the composite as a whole which does.[3]

At room temperature, the fraction of load borne by the copper matrix peaks at an applied stress approximately equal to the 0.2 pct yield stress of the unreinforced matrix, after which the fraction decreases due to plasticity in the copper matrix. One might expect the load bearing of the copper to be constant prior to macroscopic yield. The most likely explanation for changes at the low loads is a relaxation of the residual stresses present from fabrication. At high temperatures, however, not only is the efficiency of load transfer to the reinforcement reduced relative to that at room temperature, it decreases further as the load is raised, resulting in a much-higher level of load being born by the matrix. In other words, because matrix creep and stress relaxation are rapid in the matrix, it is not possible for the matrix to bear the high stress gradient required to transfer load efficiently to the reinforcement. Therefore, the reinforcement becomes less effective as the temperature is raised, until the stress borne by the matrix is the same as the applied stress. Figure 7 even shows that, at an applied stress of 125 MPa, the copper phase stress is slightly larger than the macroscopic applied stress. This might indicate that the molybdenum reinforcement has delaminated from the matrix, or that creep is so effective in the matrix surrounding

the reinforcement that no load is transferred to the reinforcement, resulting in a matrix which exhibits a smaller effective cross section. An upper bound for this effect is when no load is transferred across the particle/matrix interface and the matrix bears a higher stress of a factor of $1/(1 - f)$ times the applied stress (where f is the reinforcement volume fraction), as shown for the case of $f = 0.15$ in Figure 7, with the dotted line marked as the "delaminated interface."

VI. CONCLUSIONS

Pulsed neutron diffraction measurements were performed *in situ* during mechanical loading of composites consisting of a copper matrix reinforced with nominally 15 vol pct elastic molybdenum particulates. Elastic strains in both phases were determined at different stresses at room temperature, where the matrix yields plastically by slip and strain hardens, and at elevated temperatures, where the matrix creeps. While FE models provide reasonably good predictions of the microscopic elastic phase strains, they overestimate the macroscopic elasto-plastic strain (and correspondingly, underestimate the strength) of the composites. This discrepancy is primarily attributed to the complex structure of the molybdenum particulates, which contain a continuous copper phase and, thus, contribute to strong matrix strain hardening. The load transfer from the matrix to reinforcement is both qualitatively and quantitatively different in the two temperature regimes. When the matrix creeps, load transfer is much-less effective than when the matrix deforms by slip, and it also becomes less effective as the applied stress is raised.

ACKNOWLEDGMENTS

The Lujan Center is a national user facility funded by the United States Department of Energy, Office of Basic Energy Science and Defense Programs. This work was supported in part under DOE Contract No. W-7405-ENG-36 with the University of California. We also acknowledge useful discussions with Dr. A. Wanner (Stuttgart University) concerning the microstructure of Cu/Mo particulates in the composites.

REFERENCES

1. T.W. Clyne and P.J. Withers: *An Introduction to Metal Matrix Composites*, Cambridge University Press, Cambridge, United Kingdom, 1993.
2. D.C. Dunand and B. Derby: in *Fundamentals of Metal Matrix Composites*, S. Suresh, A. Mortensen, and A. Needleman, eds., Butterworth-Heinemann, Boston, MA, 1993, pp. 191-214.
3. P.J. Withers, W.M. Stobbs, and O.B. Pedersen: *Acta Metall. mater.*, 1989, vol. 37, pp. 3061-84.
4. A. Levy and J.M. Papazian: *Metall. Trans. A*, 1990, vol. 21A, pp. 411-20.
5. A.J. Allen, M.T. Hutchings, C.G. Windsor, and A. Andreani: *Adv. Phys.*, 1985, vol. 34, pp. 445-73.
6. M.A.M. Bourke, J.A. Goldstone, M.G. Stout, A.C. Lawson, and J.E. Allison: in *Residual Stresses in Composites: Modelling, Measurement and Effects on Thermomechanical Properties*, E.V. Barrera and I. Dutta, eds., TMS, Warrendale, PA, 1993, pp. 67-77.
7. M.A.M. Bourke, J.A. Goldstone, N. Shi, J.E. Allison, M.G. Stout, and A.C. Lawson: *Scripta Mater.*, 1993, vol. 29, pp. 771-776.
8. N. Shi, M.A.M. Bourke, J.A. Roberts, and J.E. Allison: *Metall. Mater. Trans. A*, 1997, vol. 28A, pp. 2741-53.
9. M.R. Daymond and P.J. Withers: *Scripta Metall.*, 1996, vol. 35, pp. 717-20.
10. M.R. Daymond and P.J. Withers: *Appl. Comp. Mater.*, 1997, vol. 4, pp. 377-94.
11. P.R. Subramanian and D.E. Laughlin: *Bull. Alloy Phase Diagrams*, 1990, vol. 11.
12. C. Lund: Master's Thesis, MIT, Cambridge, MA, 1997.
13. J.D. Eshelby: *Proc. R. Soc.*, 1957, vol. A241, pp. 376-96.
14. A. Wanner and D.C. Dunand: MIT, Cambridge, MA, unpublished research, 1999.
15. H.P. Cheskis and R.W. Heckel: *Metal Matrix Composites*, ASTM STP 438, ASTM, Philadelphia, PA, 1968, vol. 1, pp. 76-91.
16. I.C. Noyan and J.B. Cohen: *Residual Stress–Measurement by Diffraction and Interpretation*, Springer-Verlag, New York, NY, 1987.
17. G.E. Bacon: *Neutron Diffraction*, 3rd ed., Clarendon, Press, Oxford, United Kingdom, 1975.
18. M.R. Daymond and P.J. Withers: *Scripta Mater.*, 1996, vol. 35, pp. 1229-34.
19. H.M. Rietveld: *J. Appl. Cryst.*, 2, 65-71 (1969).
20. R.B. Von Dreele, J.D. Jorgensen, and C.G. Windsor: *J. Appl. Cryst.*, 1982, vol. 15, pp. 581-89.
21. M.R. Daymond, M.A.M. Bourke, R.B. Von Dreele, B. Clausen, and T. Lorentzen: *J. Appl. Phys.*, 1997, vol. 82, pp. 1554-62.
22. M.R. Daymond, M.A.M. Bourke, and R.B. Von Dreele: *J. Appl. Phys.*, 1999, vol. 85, pp. 739-47.
23. A.C. Larson and R.B. Von Dreele: "GSAS–General Structure Analysis System," Report No. LAUR 86-748, Los Alamos National Laboratory, Los Alamos, NM, 1994.
24. A. Colclough, B. Dempster, Y. Favry, and D. Valentin: *Mater. Sci. Eng.*, 1991, vol. A135, pp. 203-07.
25. H.M.A. Winand: Ph.D. Thesis, University of Cambridge, Cambridge, United Kingdom, 1996.
26. H.D. Hibbitt, B.I. Karlsson, and A. Sorensen: *5.4 ed.*, HKS(UK) Ltd., Pawtucket, RI, 1994.
27. *5.0 ed.*, MacNeal-Schwendler Corp., Los Angeles, CA, 1996.
28. G. Bao, J.W. Hutchinson, and R.M. McMeeking: *Acta Metall. Mater.*, 1991, vol. 39, pp. 1871-82.
29. M.R. Daymond and P.J. Withers: *Mater Sci. Technol.*, 1995, vol. 11, pp. 228-36.
30. A. Levy and J.M. Papazian: *Acta Metall. Mater.*, 1991, vol. 39, pp. 2255-66.
31. O.C. Zienkiewicz: *The Finite Element Method*, McGraw-Hill, Maidenhead, United Kingdom, 1986.
32. *Metals Handbook*, 9th ed., H. Baker and D. Benjamin, eds., ASM, Metals Park, OH, 1980, vol. 2.
33. H.E. Boyer: *Atlas of Stress-Strain Curves*, ASM INTERNATIONAL, Metals Park, OH 1987.
34. H.J. Frost and M.F. Ashby: *Deformation-Mechanism Maps*, Pergamon Press, Oxford, 1983.
35. P.E. Krajewski, J.E. Allison, and J.W. Jones: *Metall. Trans. A*, 1993, vol. 24A, pp. 2731-41.
36. *Free Energy of Formation of Binary Compounds: An Atlas of Charts for High-Temperature Chemical Calculations*, T.B. Reed, ed., MIT Press, Cambridge, MA, 1971.
37. *Binary Alloy Phase Diagrams*, T.B. Massalski, ed., ASM INTERNATIONAL, Materials Park, OH. 1990.
38. L.M. Brown and W.M. Stobbs: *Phil. Mag.*, 1971, vol. 23, pp. 1185-99.
39. A. Mortensen, O. B. Pedersen, and H. Lilholt: *Scripta Mater.*, 1998, vol. 38, pp. 1109-15.
40. E. Arzt: *Res. Mech.*, 1991, vol. 31, 399-453.
41. G.E. Dieter: *Mechanical Metallurgy*, McGraw-Hill, New York, NY, 1986.
42. C.J. Smithels: *Metals Reference Book*, Butterworth-Heineman, Boston, MA, 1992.